SPATIAL DISTRIBUTION AND MORPHOLOGY OF CRATERS ON RYUGU: IMPLICATIONS FOR SURFACE PROCESSES ON THE C-TYPE ASTEROID. Y. Cho[1], T. Morota[2], M. Kanamaru[3], C. M. Ernst[4], O. S. Barnouin[4], E. Tatsumi[1], M. Hirabayashi[5], K. A. Otto[6], N. Schmitz[6], R. J. Wagner[6], R. Jaumann[6], H. Miyamoto[1], H. Kikuchi[1], R. Hemmi[1], R. Honda[7], S. Kameda[8], Y. Yokota[9], T. Kouyama[10], H. Suzuki[11], M. Yamada[12], N. Sakatani[9], C. Honda[13], M. Hayakawa[9], K. Yoshioka[1], M. Matsuoka[9], T. Michikami[14], N. Hirata[15], H. Sawada[9] and S. Sugita[1]. [1]The University of Tokyo (7-3-1 Hongo, Bunkyo, Tokyo, Japan, cho@eps.s.u-tokyo.ac.jp), [2]Nagoya Univ., [3]Osaka Univ., [4]JHU/APL, [5]Auburn Univ., [6]DLR Berlin, [7]Kochi Univ., [8]Rikkyo Univ., [9]ISAS/JAXA, [10]AIST, [11]Meiji Univ., [12]Chiba Inst. Tech., [13]Univ. Aizu, [14]Kindai Univ., [15]Kobe Univ.

Introduction: The asteroid 162173 Ryugu is the first C-type asteroid globally observed at a resolution higher than 2 m/pix. The telescopic optical navigation camera (ONC-T) on board the Hayabusa2 spacecraft has been acquiring images since its arrival to the target asteroid in late June, 2018 [1, 2]. This comprehensive dataset, with uniform image resolution and illumination conditions, enables detailed observations of the geology of this asteroid.

Impact craters are one of the most prominent and ubiquitous geologic features on this asteroid and provide fundamental information on the asteroidal surface, including surface ages, physical properties, and crater degradation processes. Here we update our initial reports [3, 4] regarding morphology and the distribution of craters found on the asteroid Ryugu.

Image Data: We used images obtained at multiple altitudes with varying spatial resolution to find and observe crater candidates globally. Such image sets include those acquired from altitudes of 20 km, 5 km, and 3 km. Spatial resolution of the images were 2, 0.5 and 0.3 m/pix, respectively. We also used images obtained during a campaign to observe the south pole to search for craters at high southern latitudes. Note that the available viewing geometries pose a challenge to finding craters north of 60°N. This region will be visited by another observation campaign in January 2019.

Methods: We conducted stereoscopic analyses to find circular depressions. The profiles of the craters were measured using a 800k-plate shape model [5]. We mapped numerous points on each crater rim using the Small Body Mapping Tool (SBMT). The crater diameter, *D,* was calculated as the average length of the longest and shortest axes of the ellipse that fits the data points. Then the plane that best matches the data points on the rim was derived for individual crater candidates. The distance between the best-matched plane and the lowest point in the crater was calculated to obtain the depth (*d*) of each crater. Note that the curvature due to Ryugu's shape complicates the crater shape measurements, particularly for those on the equatorial ridge. For such saddle-shaped craters, which are typically larger than 100 m, east-west profiles were derived from the shape model and used to measure dimensions.

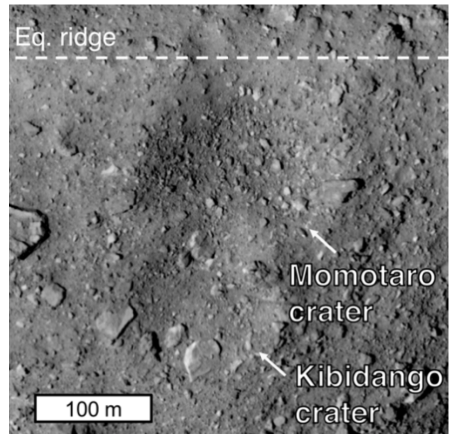

Fig. 1. Crater doublet named *Momotaro* and *Kibidango*.

Candidate Craters: Seventy crater candidates larger than 10 m have been found on Ryugu so far. They include two candidates near the south pole, which were added after our last report [3]. Craters smaller than 10 m were found as well by using high-resolution images obtained during several descending operations, but were not considered in this study.

There are 15 crater candidates larger than 100 m and 30 candidates larger than 50 m. We preliminarily defined 4 classes based on their morphologies (confidence level, CL, where CL1 represents circular depressions with sharper rims and CL4 represents quasi-circular features without apparent depressions. See [3] for details).

Morphological Features: *Urashima* is the largest (*D*~300 m) crater on Ryugu. This crater is located on the equatorial ridge. A possible slump is observed on its southeastern wall. Slightly darker material is exposed at the bottom of this crater. The nature of the dark material is being investigated, but it could be smoother material infilling from the wall, another stratigraphic layer exposed. No obvious ejecta deposit has been found around the craters larger than 50 m, consistent with the low escape velocity on this asteroid (~0.3 m/s). Nevertheless, possible ejecta deposits were observed near a few craters as small as < 10 m.

Many craters overlap with each other on Ryugu. The crater doublet named *Momotaro* (13°S, 52°E) and *Kibidango* (31°S, 50°E) is a relatively fresh-looking example (Fig. 1). The *Kibidango* crater overlies *Momotaro*.

Huge (up to ~50 m across) bright boulders are found on the crater wall of *Kibidango*. The eastern half of *Momotaro*'s floor is particularly rich in m-sized boulders of the color similar to these huge bright boulders. This could indicate that the impact that made overlying *Kibidango* broke the original rim of *Momotaro*, scattering the boulders into its floor. Understanding the mechanism responsible for the dense boulder distribution would have implications for cratering processes, material transport on and under the surface, or the relative age of craters based on the abundance of boulders on the floor.

There is a quasi-circular depression with a disturbed/modified rim at 28°N, 6°W (CL3). The concurrence of the shape of its rim and the locations of large boulders suggest that the crater excavation process was hindered by the large boulders on/under the original surface. If this is the case, this crater provides an example of cratering on a boulder-rich surface.

It might be challenging to conclude whether or not quasi-circular features (CL4), which are defined by the circular arrangement of boulders, are actually impact craters. If we assume they are, then the boulders and materials filling these craters require very efficient material transport or crater degradation processes.

Crater Shapes: The overall *d*/*D* ratio of all crater candidates was measured to be 0.07 ± 0.03, which is comparable to that reported for Itokawa [6]. The craters (CL 1-2) larger than 100 m yield a *d*/*D* of 0.11 ± 0.02, while smaller ones have a shallower *d*/*D* of 0.07 ± 0.02. *Urashima*, the largest crater on Ryugu, exhibits a *d*/*D* of 0.14. Some less-confident candidates larger than 100 m yielded much shallower values (<0.06). Moreover, the craters at the mid-to-high latitudes are more degraded than those in the equatorial region (Fig. 2): few craters deeper than a *d*/*D* of 0.1 are found in the latitudes poleward of 30°N/30°S. This result strongly suggests the presence of processes that preferentially degrade craters at mid-to-high latitudes, and/or different material properties that better preserves craters in the equatorial region. Comparing our results with those from another independent study [7] would provide a good estimate of uncertainties in the crater shape measurements.

Longitudinal Distribution of Craters: Ryugu exhibits a potential longitudinal dichotomy between the western bulge (180-300°E) and the eastern hemisphere [2]. Our crater density analysis supports the presence of the dichotomy: the eastern hemisphere has crater number (D > 30 m, CL1-2) density of 14 ± 3 km^{-2}, 2.5 times as high as that of the western bulge (5.6 ± 2.5 km^{-2}). The enhancement is significant when the Poisson errors are taken into account.

Latitudinal Distribution of Craters: The number of craters in each latitudinal strip was examined. Note that the area becomes small at higher latitudes because of Ryugu's top shape. For example, the latitudinal belts poleward of 40°S or 40°N account for only 33% of Ryugu's surface area. Our results indicate that the circular depressions (CL1, 2) are more densely distributed on the equatorial region than at the middle-to-high latitudes, even when the area of each strip is corrected (Fig. 3). This result supports the efficient crater erasure process at the mid-to-high latitudes and/or different material properties there, consistent with other morphological evidence described above.

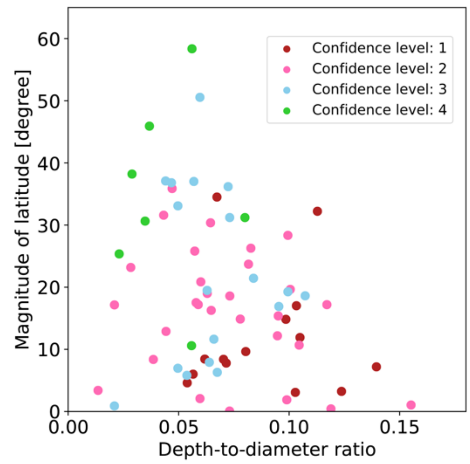

Fig. 2. Crater *d*/*D* vs. latitude. Only shallow craters are found higher than 30°.

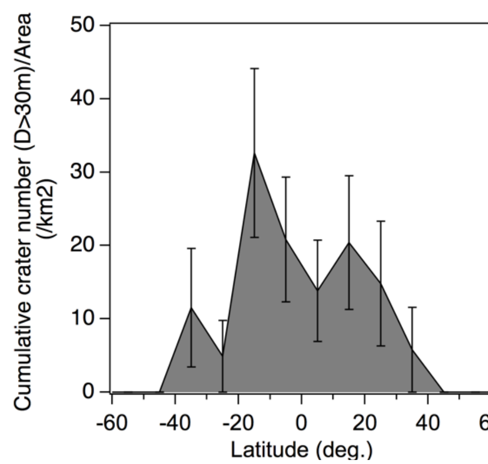

Fig. 3. Crater number density vs. latitude. Craters are concentrated around the low latitudes. Error bars indicate the square root of crater number in each bin.

References: [1] Kameda S. et al. (2017) *SSR* 208, 17. [2] Sugita S. et al. *Science*, in revision [3] Cho Y. et al. (2018) *AGU*, #377432 [4] Morota T. et al. (2018) *AGU*, #416730 [5] Hirata N. et al. (2018) *AGU*, #431018. [6] Hirata et al. (2009) *Icarus*, *200*, 486-502. [7] Ernst et al. (2019) *this meeting*.